Supporting Information

Femtosecond X-ray Liquidography Visualizes Wavepacket Trajectories in Multidimensional Nuclear Coordinates for a Bimolecular Reaction

Jong Goo Kim,[1,2,3] *Eun Hyuk Choi,*[1,2,3] *Yunbeom Lee,*[1,2,3] *and Hyotcherl Ihee*[1,2,3]*

[1]Department of Chemistry, KAIST, Daejeon 34141, Republic of Korea

[2]KI for the BioCentury, KAIST, Daejeon 34141, Republic of Korea

[3]Center for Nanomaterials and Chemical Reactions, Institute for Basic Science (IBS), Daejeon 34141, Republic of Korea

*Correspondence to: hyotcherl.ihee@kaist.ac.kr

1. Time-resolved x-ray liquidography experiment on $[Au(CN)_2^-]_3$

Time-resolved x-ray liquidography (TRXL) is an experimental technique suited for investigating structural dynamics of various molecules ranging from small molecules to macromolecules such as proteins in solution. The technique utilizes a pump-probe scheme by employing a laser pump pulse for initiating photoinduced structural dynamics of molecules and an x-ray probe pulse for detecting structural changes involved in the photoinduced reaction. A schematic of TRXL experiment is shown in Figure S1. Since x-ray scatter off all atomic pairs in a molecule, an x-ray scattering signal is sensitive to three-dimensional molecular structure, making it a complementary experimental tool to conventional time-resolved spectroscopic methods, which are sensitive to rather energetic information than molecular geometry.

TRXL experiments were performed for the sample solution of a gold trimer complex (GTC), $[Au(CN)_2^-]_3$, at the XSS beamline of PAL-XFEL, the BL3 beamline of SACLA, and the NW14A beamline of KEK. The details of experimental parameters are described in our previous publications.[1,2] Briefly, the sample solution of $[Au(CN)_2^-]_3$ was excited by a 100-fs laser pulse at the wavelength of 267 nm, and a time-delayed x-ray pulse was used to probe the structural change accompanied during the reaction. The x-ray scattering patterns were measured with an area detector (Rayonix MX225-HS). The laser-on images were measured at various time delays. The laser-off images were acquired with the x-ray pulse arriving 20 ps earlier than the laser pulse (that is, –20 ps time delay) and subtracted from the laser-on images to yield time-resolved difference scattering patterns. In the aqueous solution of $Au(CN)_2^-$ at 300 mM concentration used in this work, consideration for the relative abundance, the relative absorbance, and the relative magnitude of a difference scattering curve, the contribution from $[Au(CN)_2^-]_3$ trimers to the difference scattering curve is dominant over those from monomers and dimers.[1,2]

2. Sensitivity map

The need for and concept of the sensitivity map

The TRXL signal is directly sensitive to the three-dimensional structure of a molecule and is determined by the position of constituent atoms or the interatomic distances in the molecule. If it is possible to predict which atomic positions or interatomic distances will contribute to the TRXL signal predominantly, we can assess the applicability and suitability of TRXL method to study the structural dynamics of the molecule of interest before conducting an experiment. The sensitivity of the TRXL signal to the atomic position or internuclear distance was evaluated by quantifying the degree of change in the difference scattering curve upon the change of the atomic position or internuclear distance. First, the reference difference scattering curve ($\Delta S_{\mathrm{ref}}(q)$) arising from a reaction of interest (for example, the change from a reactant to a product) is calculated. Compared to the reference difference scattering curve, the degree of change in the difference scattering curve upon the modification of the atomic position or interatomic distance of the participating molecules (for example, a reactant and a product) is evaluated as described in the following.

Sensitivity to the atomic position

To evaluate the sensitivity to the atomic position, each atom is shifted spherically from its reference position using the evenly spaced coordinates generated by the spiral method. In detail, the position of the atom is translated by $r_j(R,\theta_j,\varphi_j)$, which is the j th coordinate of the spiral of a sphere with radius R. The j th coordinate of the spiral of the sphere is given by

$$\theta_j = \arccos\left(\frac{2j-1-J}{J}\right) \tag{S1}$$

$$\varphi_j = \sqrt{\pi J}\,\arcsin\left(\frac{2j-1-J}{J}\right) \tag{S2}$$

, where J is the total number of the coordinates on the spiral of the sphere and j = 1, 2, …, J. R of 0.1 Å and J of 300 were used for this simulation. The dissimilarity between the reference difference scattering curve and the difference scattering curve calculated from the modified

structure, in which an atom is translated by r_j ($\Delta S_j(q)$), is quantified by defining the degree of change, D_j, as follows.

$$D_j = \sqrt{\sum_q (\Delta S_{\mathrm{ref}}(q) - \Delta S_j(q))^2} \tag{S3}$$

This process is iterated over all J coordinates on the spiral. The sensitivity to the atomic position of the atom is obtained by taking the mean of the D_j s. The sensitivities to the atomic positions are scaled to yield the relative sensitivities by setting the maximum sensitivity for the atomic position to be unity. The relative sensitivities of atomic positions are shown by the radii of circles, where the larger radius represents the higher sensitivity of the atomic position.

Sensitivity to the internuclear distance

The sensitivity to the internuclear distance is evaluated in a similar way to that used for evaluating the sensitivity to atomic position. To estimate the sensitivity of each internuclear distance, a modified structure is generated by elongating or contracting the internuclear distance by 0.1 Å from the equilibrium distance, while the other internuclear distances are fixed to the reference distances determined from the structural analysis. Then, dissimilarity between the reference difference scattering curve and the difference scattering curve calculated from the modified structure, of which an internuclear distance is changed, ($\Delta S(q)$) is quantified by Δ defined as follows.

$$\Delta = \sqrt{\sum_q (\Delta S_{\mathrm{ref}}(q) - \Delta S(q))^2} \tag{S4}$$

The sensitivity of internuclear distance is obtained by taking the mean of Δ's calculated from the modified structures generated by the elongation or contraction of the internuclear distance. The sensitivities of the interatomic distances are scaled to yield the relative sensitivities by setting the maximum sensitivity for the interatomic distance to be unity. The relative

sensitivities of the interatomic distances are shown by the color gradient of lines, where the darker color represents the higher sensitivity of the interatomic distance.

Sensitivity map for the bond formation reaction of GTC

To obtain the sensitivity map for the bond formation reaction of GTC shown in Figure 2, we considered the structural difference between the equilibrium structures of S_0 and T_1', determined by the structural analysis using the TRXL data to obtain the reference difference scattering curve. We calculated the relative sensitivities to the atomic positions and interatomic distances in GTC following the procedures described above.

The comparison of the two types of parameters provides an interesting insight. For example, since R_{12} and R_{23} of T_1' correspond to the distance of Au–Au pairs, it is expected to predominantly contribute to the TRXL signal, and this is true as shown in Figure 2. From these observations, one might guess that the position of Au_2 should contribute to the signal the most, since the position of Au_2 affects both R_{12} and R_{23}. However, the position of Au_2 is not quite sensitive to the signal as can be seen from the small circle for Au_2 in Figure 2. This insensitivity arises because the structure of T_1' is linear and symmetric. When Au_2 moves closer to Au_1, the distance to Au_3 increases conversely. Accordingly, the contributions arising from the decrease of R_{12} and increase of R_{23} cancel out each other.

3. Quantum mechanical description for the wavepacket dynamics in TRXL signals

Vibrational wavepacket dynamics in most of the fs-TRXL data including those of $[Au(CN)_2^-]_3$ solution have been interpreted in a semi-classical picture.[1,3,4] Here, we briefly summarize a quantum mechanical formalism for the time-resolved x-ray scattering signals following the theoretical framework by Mukamel. More detailed and rigorous description can be found in literature.[5-7] Also, different approaches and formalisms by other groups can be found elsewhere.[8-10] Although the formalisms are assuming gas phase molecules, the basic principle will be shared for the liquid phase system.

The time-dependent molecular wave function at a nuclear coordinate $\boldsymbol{R}$ and time t, $\left|\psi(\boldsymbol{R},t)\right\rangle$, can be expanded in the adiabatic electronic eigenstates, $\left|\phi_i\right\rangle$, and time-dependent nulcear wavepackets, $\left|\chi_i(\boldsymbol{R},t)\right\rangle$, on the electronic state $\left|\phi_i\right\rangle$, as follows

$$\left|\psi(\boldsymbol{R},t)\right\rangle = \sum_i c_i(t)\left|\chi_i(\boldsymbol{R},t)\right\rangle \otimes \left|\phi_i\right\rangle \tag{S5}$$

where $c_i(t)$ is the amplitude of the electronic state and $\otimes$ denotes tensor product.

The x-ray scattering signal at a time delay T, $S(\boldsymbol{q}, \mathrm{T})$, is given by the following expression

$$\begin{aligned} S(\boldsymbol{q},\mathrm{T}) &= N\int dt \left|E_p(t-T)\right|^2 \left\langle \psi(\boldsymbol{R},t)\left|\hat{\sigma}^\dagger(\boldsymbol{q})\hat{\sigma}(\boldsymbol{q})\right|\psi(\boldsymbol{R},t)\right\rangle \\ &= N\int dt \left|E_p(t-T)\right|^2 \sum_{ijk} \rho_{ij}(t)\left\langle \chi_i(\boldsymbol{R},t)\left|\hat{\sigma}_{ik}^\dagger(\boldsymbol{q})\hat{\sigma}_{kj}(\boldsymbol{q})\right|\chi_j(\boldsymbol{R},t)\right\rangle \end{aligned} \tag{S6}$$

where N is the number of active molecules, the indices i, j and k refer to the vibronic states, $E_p(t)$ is the temporal envelope of the x-ray pulse, ρ_{ij} is the i,j-th element of the density matrix of the electronic state and $\hat{\sigma}(\boldsymbol{q})$ is the spatial Fourier transform of the electronic charge-density operator, where $\hat{\sigma}_{ij}(\boldsymbol{q})$ denotes $\left\langle \phi_i\left|\hat{\sigma}(\boldsymbol{q})\right|\phi_j\right\rangle$. This equation involves elastic, inelastic, and mixed elastic-inelastic scattering components. For example, among the various contributions in the above equation, one of the signals originating from the ground state wavepacket (S_{GWP}) correspond to the following term.

$$S_{\mathrm{GWP}}(\boldsymbol{q},\mathrm{T}) = N\int dt \left|E_p(t-T)\right|^2 \rho_{\mathrm{g'g}}\left\langle \chi_{\mathrm{g'}}(\boldsymbol{R},t)\left|\hat{\sigma}_{\mathrm{g'g}}^\dagger(\boldsymbol{q})\hat{\sigma}_{\mathrm{gg}}(\boldsymbol{q})\right|\chi_{\mathrm{g}}(\boldsymbol{R},t)\right\rangle \tag{S7}$$

where g and g' denote the vibrationally ground and excited state of the ground electronic state, respectively. This term corresponds to a signal from coherent superposition of vibrational states on the ground electronic state via impulsive stimulated Raman scattering (ISRS) during the interaction with the optical pump pulse.

4. Assignment of normal modes of the ground and excited-state wavepackets

To identify the origin of the oscillations observed in $q\Delta S_{\text{residual}}(q,t)$, we fitted the time-dependent structural parameters of S_0 and T_1' in the late time range (> 360 fs). The detailed procedures are described in our previous publication.[1] The procedures are summarized briefly in the following.

To assign the vibrations of T_1' to specific vibrational normal modes, we fitted $R_{12}(t)$, $R_{23}(t)$, and $R_{13}(t)$, of T_1', in the late time range, using a sum of damping cosine functions. Specifically, time-dependent Au–Au distances were described by a sum of damping cosine functions, ${R_{12}}^{thy}(t)$, ${R_{23}}^{thy}(t)$, and ${R_{13}}^{thy}(t)$ as follows:

$$\begin{aligned} {R_{12}}^{thy}(t) &= {R_{12}}^{T_1',eq} + \sum_i^n A_i \cos(2\pi c t \nu_i + \phi_i)\exp(-t/\tau_i) \\ {R_{23}}^{thy}(t) &= {R_{23}}^{thy}(t) \\ {R_{13}}^{thy}(t) &= 2{R_{13}}^{thy}(t) \end{aligned} \qquad \text{(S8)}$$

where ${R_{12}}^{T_1',eq}$ is the R_{12} in the equilibrium structure of T_1', A_i, ν_i, ϕ_i, and τ_i are the amplitude, frequency, phase, and damping constant of a damping cosine function, respectively, and n is the number of damping cosine functions used for the fitting. The discrepancy between the experimentally-resolved Au–Au distances of T_1', and the theoretical Au–Au distances calculated by Eq. (S8), ${R_{12}}^{thy}(t)$, ${R_{23}}^{thy}(t)$, and ${R_{13}}^{thy}(t)$, was minimized by adjusting fitting parameters (A_i, ϕ_i, and τ_i). The satisfactory fits shown in Figure 4d were obtained using two damping cosine functions (that is, n = 2 in Eq. (S8)) with 79 cm^{-1} and 125 cm^{-1} frequencies. Therefore, the symmetric stretching vibrations of T_1' correspond to two symmetric stretching modes (T_1_#6 and T_1_#12, where the numbers indicate the order of appearance in the DFT frequencies of T_1)[1] with the 79 cm^{-1} and 125 cm^{-1} frequencies.

For S_0, we performed another type of fitting analysis using displacement vectors of candidate normal modes to identify the ground-state wave packets created in S_0 as follows. In principle, the time-dependent Au–Au distances of S_0 can be described by a combination of normal modes obtained from DFT calculation for S_0. Specifically, the time-dependent Au–Au

distances, $R_{12}(t)$, $R_{23}(t)$, and $R_{13}(t)$, of S_0 were fit by theoretical Au–Au distances that were constructed with a combination of displacement vectors of candidate normal modes.

To calculate the theoretical Au–Au distances described by the normal mode vibrations, $R_{12}^{NM}(t)$, $R_{23}^{NM}(t)$, and $R_{13}^{NM}(t)$, we assumed that the structure of S_0 vibrates following the displacement vectors of candidate normal modes modeled to damp exponentially. As a result, time-dependent structure of S_0 was described as follows,

$$R_{S_0}{}^{NM}(t) = R_{S_0{}^{eq}} + \sum_{i}^{N} D_{NM_i} A_{NM_i} \cos(2\pi c t \nu_{NM_i} + \phi_{NM_i}) \exp(-t/\tau_{NM_i}) \quad \text{(S9)}$$

where $R_{S_0}{}^{NM}(t)$ and $R_{S_0{}^{eq}}$ are 3×3 matrices whose row vectors are three-dimensional coordinates that indicate the positions of the three Au atoms at *t* and in the equilibrium structure of S_0, respectively, D_{NM_i} is a 3×3 matrix whose row vectors are three-dimensional displacement vectors of the three Au atoms for each normal mode, A_{NM_i} is the scaling factor for the vibrational amplitude of each mode, ν_{NM_i} is the oscillating frequency of each mode, ϕ_{NM_i} is the phase of each mode, τ_{NM_i} is the damping time constant of each mode, *c* is the speed of light, and *N* is the number of normal modes used for the fitting. Using the three-dimensional coordinates of Au atoms in a transient molecular structure of S_0, $R_{S_0}{}^{NM}(t)$, described by Eq. (S9), Au–Au distances changed by normal mode vibrations, $R_{12}^{NM}(t)$, $R_{23}^{NM}(t)$, and $R_{13}^{NM}(t)$, were calculated.

The discrepancy between the experimentally-determined Au–Au distances of S_0, and the theoretical Au–Au distances described by the normal mode vibrations was minimized by adjusting fitting parameters (A_{NM_i}, ν_{NM_i}, ϕ_{NM_i}, and τ_{NM_i}). The satisfactory fits shown in Figure 4f were obtained using two normal modes of S_0 (*N* = 2 in Eq. (S9)). Among all the possible combinations, the best fits to $R_{12}(t)$, $R_{23}(t)$, and $R_{13}(t)$ of S_0 were obtained when using a symmetric stretching mode (S_0_#6) and an asymmetric stretching mode (S_0_#5), of which the oscillation frequencies were determined to be 32 cm^{-1} and 44 cm^{-1}, respectively. The numbers

of S_0_#6 and S_0_#5 represent the order of the order of appearance in the DFT frequencies of S_0.[1] Thus, we concluded that a symmetric stretching mode with 32 cm^{-1} frequency and an asymmetric stretching mode with 44 cm^{-1} frequency are the active ground-state wave packets in S_0.

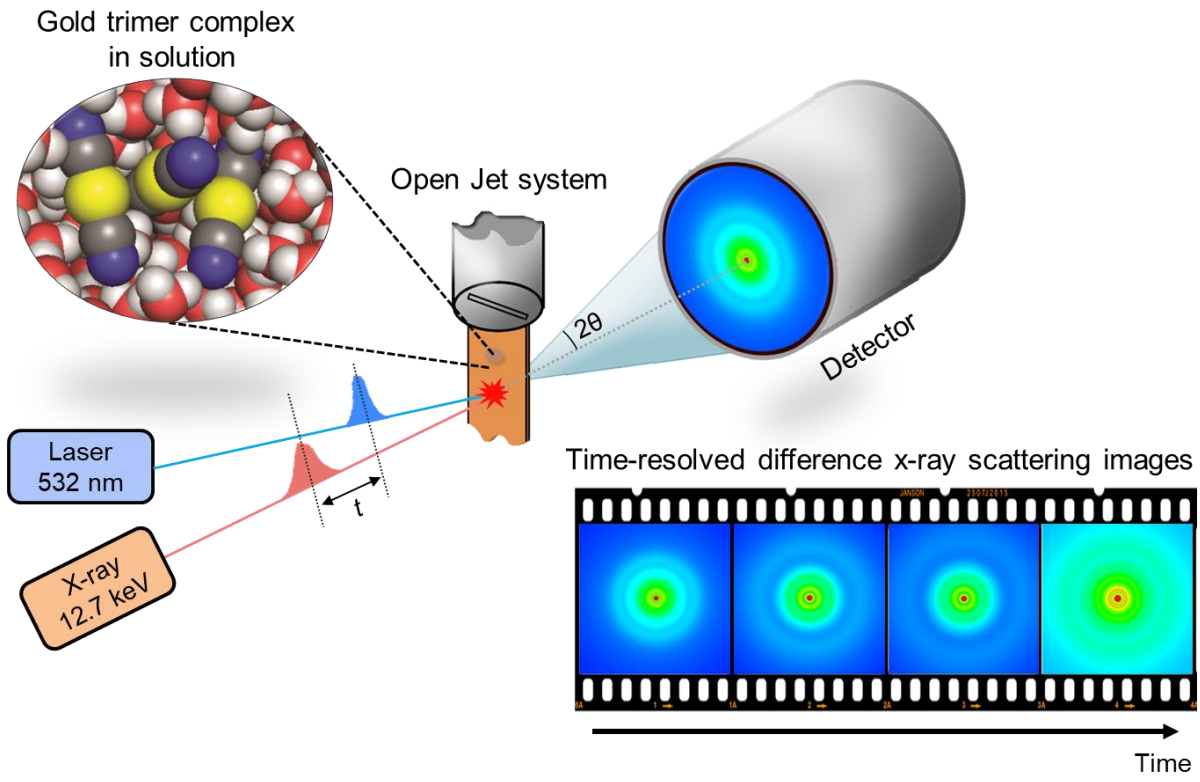

Figure S1. Schematic of TRXL experiment. The solution sample is excited by a laser (pump) pulse. An x-ray (probe) pulse is delivered with a certain time delay to track the structural change during the reaction. Time-resolved difference x-ray scattering images are obtained at various time delays to visualize the structural change in real time. 2θ is the scattering angle and *t* is a time delay between laser and x-ray pulses.

References

1. Kim, J. G.; Nozawa, S.; Kim, H.; Choi, E. H.; Sato, T.; Kim, T. W.; Kim, K. H.; Ki, H.; Kim, J.; Choi, M.; Lee, Y.; Heo, J.; Oang, K. Y.; Ichiyanagi, K.; Fukaya, R.; Lee, J. H.; Park, J.; Eom, I.; Chun, S. H.; Kim, S.; Kim, M.; Katayama, T.; Togashi, T.; Owada, S.; Yabashi, M.; Lee, S. J.; Lee, S.; Ahn, C. W.; Ahn, D. S.; Moon, J.; Choi, S.; Kim, J.; Joo, T.; Kim, J.; Adachi, S. I.; Ihee, H. Mapping the emergence of molecular vibrations mediating bond formation. *Nature* **2020**, *582*, 520-524.
2. Kim, K. H.; Kim, J. G.; Nozawa, S.; Sato, T.; Oang, K. Y.; Kim, T. W.; Ki, H.; Jo, J.; Park, S.; Song, C.; Sato, T.; Ogawa, K.; Togashi, T.; Tono, K.; Yabashi, M.; Ishikawa, T.; Kim, J.; Ryoo, R.; Kim, J.; Ihee, H.; Adachi, S.-i. Direct observation of bond formation in solution with femtosecond X-ray scattering. *Nature* **2015**, *518*, 385-389.
3. Haldrup, K.; Levi, G.; Biasin, E.; Vester, P.; Laursen, M. G.; Beyer, F.; Kjaer, K. S.; van Driel, T. B.; Harlang, T.; Dohn, A. O.; Hartsock, R. J.; Nelson, S.; Glownia, J. M.; Lemke, H. T.; Christensen, M.; Gaffney, K. J.; Henriksen, N. E.; Moller, K. B.; Nielsen, M. M. Ultrafast X-Ray Scattering Measurements of Coherent Structural Dynamics on the Ground-State Potential Energy Surface of a Diplatinum Molecule. *Phys. Rev. Lett.* **2019**, *122*, 063001.
4. Biasin, E.; van Driel, T. B.; Kjær, K. S.; Dohn, A. O.; Christensen, M.; Harlang, T.; Chabera, P.; Liu, Y.; Uhlig, J.; Pápai, M.; Németh, Z.; Hartsock, R.; Liang, W.; Zhang, J.; Alonso-Mori, R.; Chollet, M.; Glownia, J. M.; Nelson, S.; Sokaras, D.; Assefa, T. A.; Britz, A.; Galler, A.; Gawelda, W.; Bressler, C.; Gaffney, K. J.; Lemke, H. T.; Møller, K. B.; Nielsen, M. M.; Sundström, V.; Vankó, G.; Wärnmark, K.; Canton, S. E.; Haldrup, K. Femtosecond X-Ray Scattering Study of Ultrafast Photoinduced Structural Dynamics in Solvated $[Co(terpy)_2]^{2+}$. *Phys. Rev. Lett.* **2016**, *117*, 013002.
5. Bennett, K.; Biggs, J. D.; Zhang, Y.; Dorfman, K. E.; Mukamel, S. Time-, frequency-, and wavevector-resolved x-ray diffraction from single molecules. *J. Chem. Phys.* **2014**, *140*, 204311.
6. Kowalewski, M.; Bennett, K.; Mukamel, S. Monitoring nonadiabatic avoided crossing dynamics in molecules by ultrafast X-ray diffraction. *Struct. Dyn.* **2017**, *4*, 054101.
7. Bennett, K.; Kowalewski, M.; Rouxel, J. R.; Mukamel, S. Monitoring molecular nonadiabatic dynamics with femtosecond X-ray diffraction. *Proc. Natl. Acad. Sci. U.S.A.* **2018**, *115*, 6538-6547.
8. Simmermacher, M.; Henriksen, N. E.; Moller, K. B.; Carrascosa, A. M.; Kirrander, A. Electronic Coherence in Ultrafast X-Ray Scattering from Molecular Wave Packets. *Phys. Rev. Lett.* **2019**, *122*, 073003.
9. Dixit, G.; Vendrell, O.; Santra, R. Imaging electronic quantum motion with light. *Proc. Natl. Acad. Sci. U.S.A.* **2012**, *109*, 11636-11640.
10. Kirrander, A.; Saita, K.; Shalashilin, D. V. Ultrafast X-ray Scattering from Molecules. *J. Chem. Theory Comput.* **2016**, *12*, 957-967.